Measurement and Prediction of Traffic-Induced Turbulence and Velocity Fields Near Roadways

ROBERT E. ESKRIDGE[1]

Environmental Science Research Laboratory, U.S. Environmental Protection Agency, Research Triangle Park, NC 27711

S. TRIVIKRAMA RAO

Division of Air, New York State Department of Environmental Conservation, Albany, NY 12233

(Manuscript received 6 July 1982, in final form 20 April 1983)

ABSTRACT

The primary objectives of this investigation are to determine the temporal and spacial resolution needed to adequately measure vehicle wake turbulence and the characteristics of turbulence near roadways using the knowledge gained in the General Motors (GM) Sulfate Dispersion Experiment, the Long Island (LI) Expressway Diffusion Experiments and wind tunnel experiments.

Observed wind velocity fluctuations at a fixed point near a roadway are due to three distinct causes: wake turbulence, ambient turbulence and the time variation in the wind velocity as a vehicle's wake passes the observation point, hereafter referred to as wake-passing effect. The wake-passing effect can be separated in the data from the ambient and vehicle wake turbulence because of the special spacing and timing of vehicles used in the GM experiment. The measured wake-passing effect is then compared with vehicle wake model predictions. The wake-passing effect, which is shown to constitute a significant portion of the measurable velocity variance near the roadway, does *not* diffuse pollutants.

In the Long Island Expressway experiment it was shown that most of the velocity variance associated with the vehicle traffic occurred at frequencies greater than 0.5 Hz. It is shown that the GM velocity data, which were recorded once per second, underestimated the velocity variance in short wavelengths and the magnitude of the wind velocity changes due to the vehicle wake.

Recommendations are made, based on wind tunnel and modeling results, as to the time resolution and vertical spacing that are necessary to resolve vehicle wake turbulence and the role of pseudoturbulence in modeling pollutant diffusion near roadways is discussed.

1. Introduction

Locally generated turbulence due to some combination of vehicle-induced drag, roughness change, and waste heat emission from a vehicle on the roadway plays a significant role in the transport and diffusion of effluents from automobiles. Early attempts to calculate pollution concentrations adjacent to highways by the use of line source models, such as the model of Zimmerman and Thompson (1975), gave unsatisfactory results because vehicle wake turbulence was poorly represented in the model formulation used. Sedefian (1977) and Rao *et al.* (1979), in studying the Long Island Expressway in New York, found that moving traffic produces an augmentation of energy in the high frequency end of the spectra and cospectra of velocity components. In cases where the wind flows across a highway with moderate to heavy traffic conditions, the augmentation of energy is seen at frequencies between 0.1 and 1.0 Hz (Rao *et al.*).

Recently, Rao and Keenan (1980) and Chock (1978a) have greatly improved the Gaussian line-source models by incorporating wake turbulence effects observed in the GM experiments. While the models of Chock, and Rao and Keenan are significant improvements over the initial models studied by Rao *et al.* (1980), they are tuned to vehicle speeds of 80 km h^{-1} and a vehicle distribution that is not typical of highway traffic.

Eskridge and Hunt (1979) and Eskridge *et al.* (1979) have developed a finite-difference model for calculating pollutant concentrations on and near a highway that incorporates a vehicle wake theory derived from a perturbation solution to the equations of motion. The wake theory was modified and verified in wind tunnel experiments by Eskridge and Thompson (1982). The major restriction of this model is the requirement that the vehicle speed be much greater than the windspeed. This is not a serious limitation; those cases in which large pollutant concentrations are expected will meet this requirement and more importantly it is valid for all vehicle speeds when the windspeed is low. This vehicle wake model is summarized in Section 4.

The GM experiment, which is discussed in Section

[1] On assignment from Department of Commerce, NOAA.

2, resulted in a high quality data base suitable for model development and testing. The velocity variance of each wind velocity component can be calculated from the wind data at various locations upwind and downwind of the roadway. These calculated values of velocity variance represent the ambient turbulence upwind of the road and total variance downwind of the road, which is the sum (see Section 4) of the ambient and wake turbulence and wake-passing effect. It should be noted that the variance of the wind velocity components calculated from an anemometer does not necessarily represent *true* turbulence. There are two well-known phenomena that must be filtered from velocity data before the turbulence or turbulent energy spectrum is determined and these are the variance in the velocity components due to gravity waves passing through the observational network and the variance due to a trend in the data. By a trend one means a steady increase or decrease in wind speed during the sampling interval. In this paper we will present evidence that wake-passing is one of the nonturbulent events present in the velocity data near a roadway which must be removed as it is a nondiffusive event.

In the GM experiment vehicles were driven in groups past a vertical plane of meteorological sensors at 29 s intervals (frequency is 0.0345 Hz). This timing and spacing of the groups of vehicles produced a distinct forcing in the fluctuating wind components near the highway and is evident in autocorrelogram and power spectra of the wind data as analyzed by Sedefian *et al.* (1981). The energy at this frequency will be shown to be due to the wake-passing effect and hence it is possible to compare the total velocity variance and various components of the observed velocity variance with model predictions. If the energy in the 29 s frequency was due to a turbulent eddy one would expect this energy to be eventually transferred to smaller sized eddies. However, if it is due to the spacing of the groups of vehicles (which passed the plane of meteorological sensors at 29 s intervals) then there is no reason to expect a transfer of energy as there is no turbulent energy at this frequency. The 29 s component is easily distinguishable from the velocity variance due to wake turbulence and it is possible to separate ambient, vehicle wake-passing velocity variance by using the 29 s wave as a marker in the observation network; the method is given in Section 3.

In Section 4, we show how wake-passing effect arises and how it is calculated in the vehicle wake model. In Section 5, model predictions are compared with the GM data. It is shown that the difference between observations and predictions is partly due to the resolution of the data. Appropriate spacial and temporal resolution required to determine vehicle wake effects are proposed based on model computations and the experiments of Eskridge and Thompson (1982).

2. General Motors sulfate dispersion experiment

The GM experiment was conducted in September and October 1975 at the GM proving grounds in Milford, Michigan. A fleet of 352 automobiles was driven on a four-lane, north–south track of 10 km length for 17 days during the morning hours. (See Cadle *et al.* (1976) for a complete description of the experiment.) Each experiment lasted 30 minutes.

The cars were driven in 16 groups of 22 vehicles (11 vehicles in each lane). The groups were spaced approximately 322 m apart with the lead cars in each group pacing the group at 80 km h^{-1}. The groups passed the tower line (see Fig. 1) at approximately 29 s intervals. This distribution gave a traffic density of 5460 cars per hour or 1365 cars per lane per hour.

Meteorological instruments and chemical samplers were located on six towers and two stands 2.4 km north of the south end of the test track. Wind velocity components from 20 Gill UVW anemometers were recorded once per second. The anemometers were located on the towers 1.5, 4.4 and 10.44 m above the surface and at 1.5 m on the two stands. Temperature data were recorded at towers 1 and 6 every 5 s using a Rosemount Model 78-0039-0023 single-element, platinum-resistance thermometers mounted in Model 43404 Gill aspirated temperature shields. The thermometers were located on towers 1 and 6 at approximately the same positions as the anemometers.

As described by Chock (1977), the test site was rather flat and covered with medium-to-long grass. Elevation varied less than 1 m within 50 m to the west and 130 m to the east of the roadway and within 80 m to the north and to the south of the instrument tower line. There were some low hills (less than 5 m higher than the test site) to the southeast, a few trees to the northwest and a low wall (2.5 m) about 100 m to the west of the test site. Table 1 summarizes the meteorological conditions for the data sets used in this paper.

3. Analysis of the 29 s wave

As noted in Section 2, the wind velocity components in the GM experiment were recorded once per second during each experiment and each experiment lasted 30 minutes. The fluctuating (along, across and vertical to the roadway) components of velocity (u', v', w') were calculated for each second in each experiment, and autocorrelations were calculated by standard techniques (Tennekes and Lumley, 1972). Figs. 2 and 3 show typical autocorrelograms for the fluctuating velocity components u', v', and w' immediately downwind of the roadway for case 293110458 with the wind nearly perpendicular to the

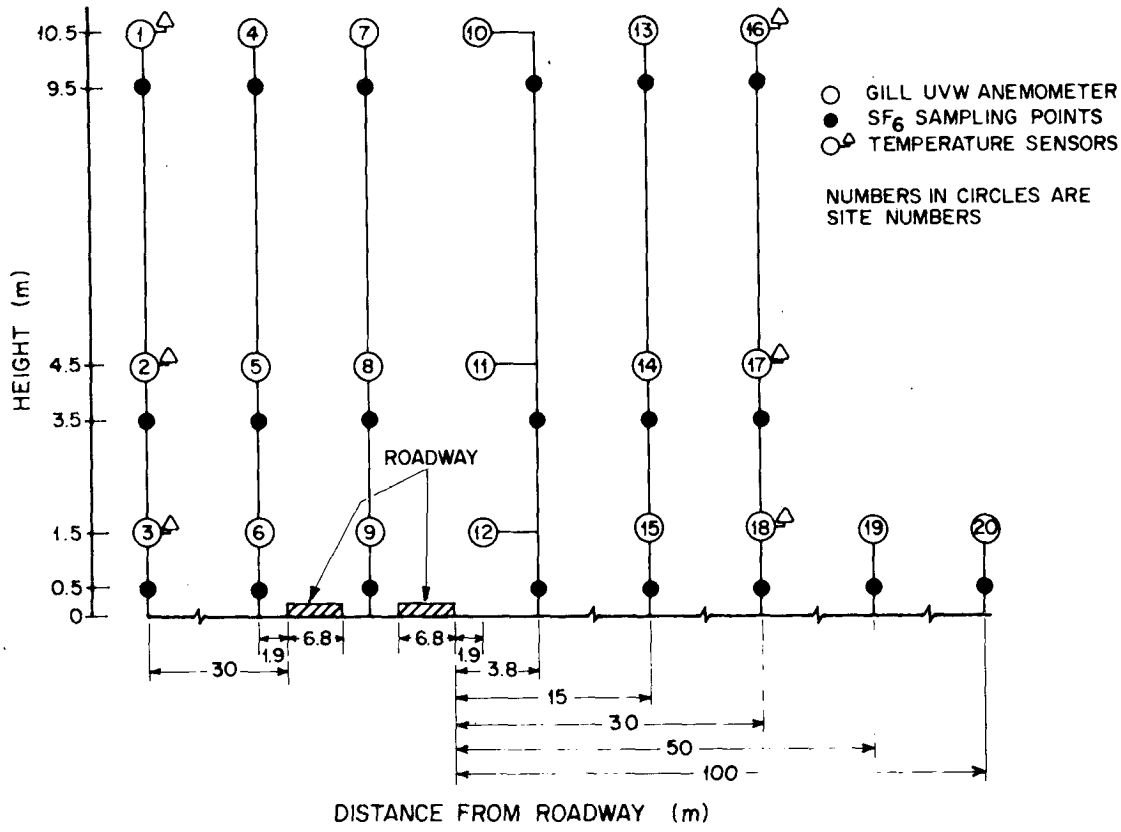

FIG. 1. Instrument layout for the GM experiment.

roadway, and case 296080500 with the wind nearly parallel to the roadway, respectively. The autocorrelations of the fluctuating wind component near the highway show a distinct 29 s oscillation for the horizontal velocity component in each case. The vertical component is small in magnitude in both cases.

When the autocorrelation shows a distinct periodicity, such as observed in Figs. 2 and 3, it is reasonable to calculate an average wave with a period, in this case, of 29 s. The average wave (denoted by a caret) is defined by

$$\hat{B}(k) = \frac{1}{N(k)} \sum_{m=1}^{N(k)} B[k + J(m-1)], \qquad (1)$$

for $k = 0, 1, 2, \ldots, 29$; where, $N(k)$ is the specific number of data points in the data block appropriate for that particular k (62 or 63), J is the period of interest (29 s), and B is the amplitude of the fluctuating velocity (u', v' or w'). The effect of averaging with (1) is to filter out all energy except that in the 29 s frequency wave.

If the velocity fluctuations are represented by only one wavelength, then for each component of the velocity variance

$$\hat{u}_i'^2 = 0.5(u_i'^2)_{\max}, \quad i = 1, 2, 3. \qquad (2)$$

Hence the velocity variance energy associated with the 29 s oscillation observed in the GM experiment q^T can be estimated by

$$q^T = \tfrac{1}{2}(\hat{u}'^2 + \hat{v}'^2 + \hat{w}'^2),$$
$$= \tfrac{1}{4}(u'^2_{\max} + v'^2_{\max} + w'^2_{\max}). \qquad (3)$$

The kinetic energy q^T can also be calculated by integrating the average waves for u', v', and w' determined by (1). However, several calculations indicate that the computed values of q^T differ by about 10% between the two methods [i.e., integrating the average waves or using (3)].

There are several possible explanations for the source of the 29 s oscillation. First, it could be ambient turbulence although the frequency is rather low. However, Fig. 4 shows that the 29 s wave is *not* observed upwind of the road, and its magnitude is greatest near the road and decreases with the distance from the road. Thus this 29 s wave does not represent ambient turbulence. Second, the 29 s oscillation could represent wake turbulence produced by the moving vehicles. The wind tunnel data of Eskridge and

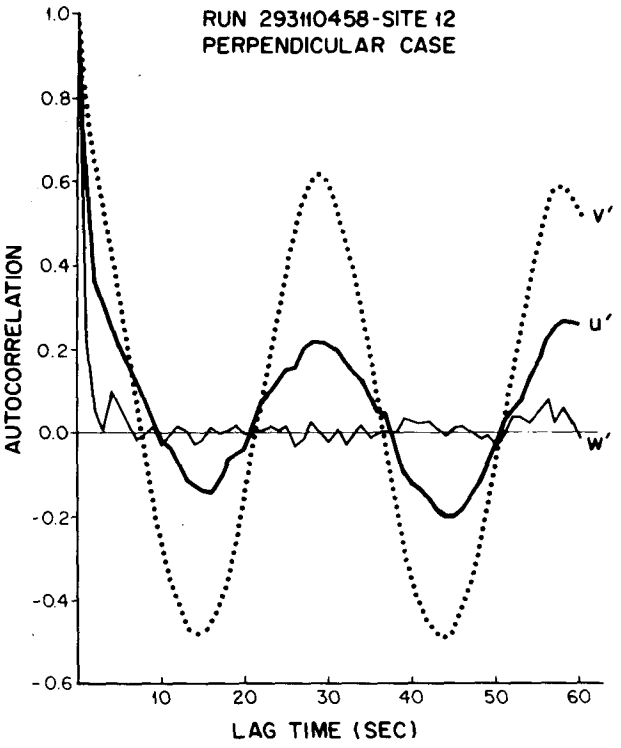

FIG. 2. A typical autocorrelogram for wind perpendicular to the road.

Thompson (1982) show from velocity spectra that wake turbulence will not contribute energy to the 29 s wave with the windspeeds shown in Table 1. Therefore, the only possible source of this energy is the time variation in the wind velocity due to the vehicle wake-passing the observation point and thus called wake-passing effect.

4. Review of vehicle wake theory

a. Single vehicle wake

The vehicle wake theory was originally developed by Eskridge and Hunt (1979) and was modified and *verified* in wind tunnel experiments by Eskridge and Thompson (1982). A brief description of those studies is given in this section.

The wake velocity deficit of a single vehicle is given by

$$u \equiv \langle u \rangle = QA\bar{s}^{-0.75} f\left(\frac{\bar{n}}{l(s)}, \frac{\bar{z}}{l(s)}\right), \qquad (4)$$

where

$$\bar{s} = s/h, \quad \bar{z} = z/(\gamma Ah), \quad \bar{n} = n/(\lambda\gamma A W_d),$$

and h is the height of the vehicle, Q is the windspeed relative to the vehicle; A is the strength of the wake determined by the overturning moment (or couple) acting on the vehicle, given by

$$A = \left[\frac{C_d}{32\pi e^{1/2}\lambda\gamma^3}\right]^{1/4}, \qquad (5)$$

where C_d is the drag coefficient; γ and λ are constants with experimentally determined (wind tunnel) values of 0.095 and 1.14, respectively; s is the coordinate along the center line of the wake; n the coordinate in the horizontal plane perpendicular to s; z the vertical coordinate (see Fig. 5); $l(s)$ is the vertical scale length of the wake and is given by $l(s) = \gamma Ah(\bar{s})^{1/4}$, and W_d is the width of the vehicle. It should also be noted that u represents an ensemble average denoted by $\langle u \rangle$.

The function f is the solution to a partial differential equation which does not have a closed form solution (see Eskridge and Thompson, 1982). However the equation is separable:

$$f\left(\frac{\bar{n}}{l(s)}, \frac{\bar{z}}{l(s)}\right) = Y\left(\frac{\bar{n}}{l(s)}\right) T\left(\frac{\bar{z}}{l(s)}\right),$$

where

$$Y\left(\frac{\bar{n}}{l(s)}\right) = C_1 \exp[-\bar{n}^2(8l^2(s))^{-1}]$$

and T is the solution (determined by numerical method)

$$H(\zeta)T''(\zeta) + \frac{\zeta}{4} T'(\zeta) + H'(\zeta)T'(\zeta) + \tfrac{1}{2}T(\zeta) = 0, \quad (6a)$$

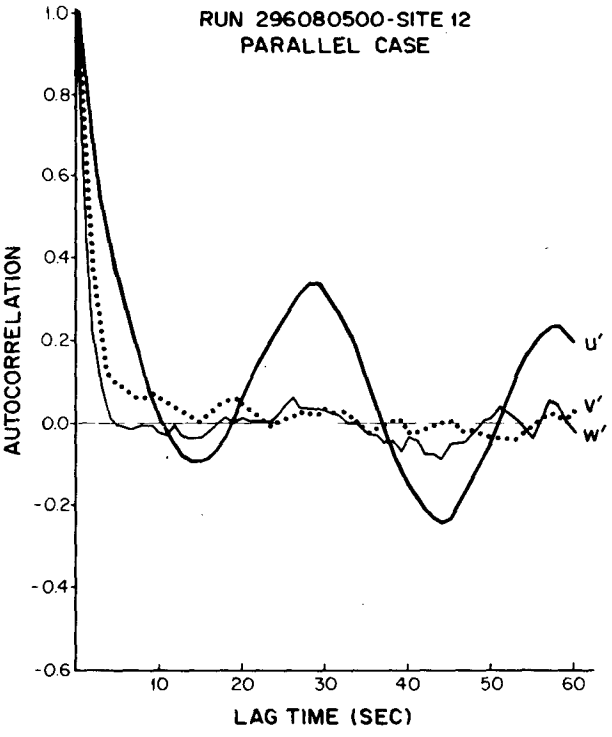

FIG. 3. As in Fig. 2 except wind parallel to the road.

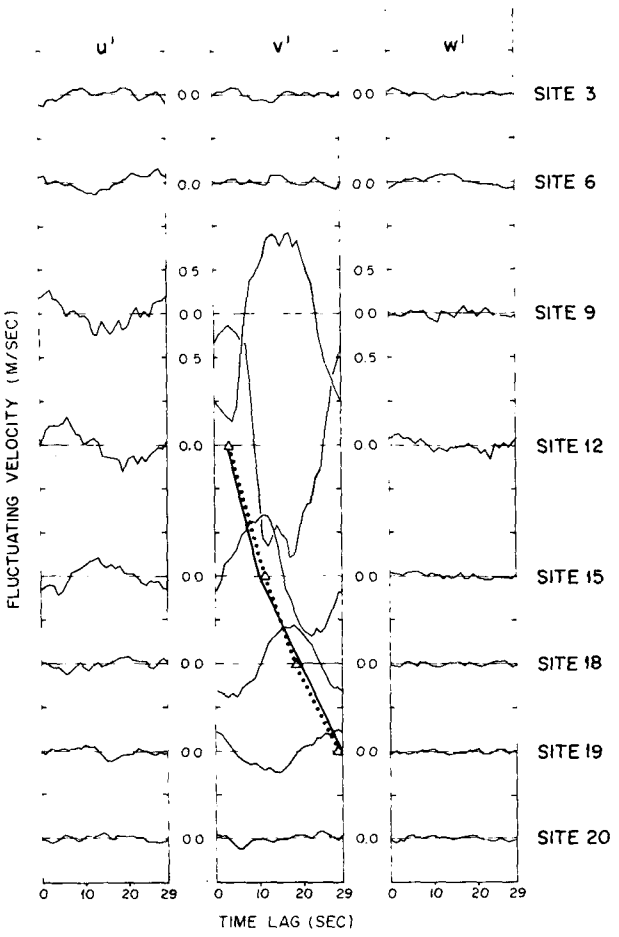

FIG. 4. The 29 s average wave at each site nearest the ground; deltas denote the location of the maximum, the dotted line is the observed phase shift, and the solid line is the calculated phase shift from the wind component normal to the road.

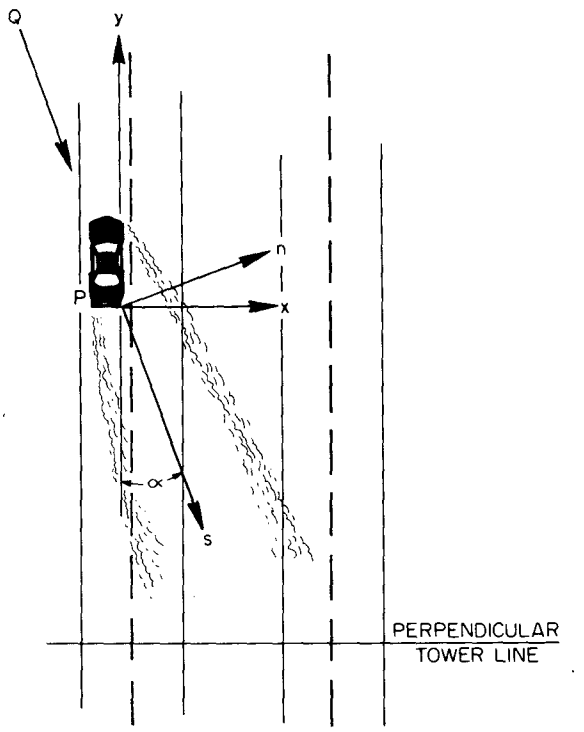

FIG. 5. The (s, n, z) system is oriented along the wake and normal to it, whereas (x, y) is fixed in the standard east–west, north–south orientation.

subject to $T(0.0) = 0.0$ and $T_{max}(\zeta) = 1.0$, where $\zeta = \bar{z}/l(s)$ and $H(\zeta)$ describes the vertical variation of eddy viscosity. (In Eskridge and Hunt, $H(\zeta)$ was a constant and f had an analytic solution.) The primes in (6a) indicate differentiation with respect to ζ.

TABLE 1. GM Data.

Case	Windspeed ($m\ s^{-1}$)	Wind direction (from true north)	Richardson number	u_* ($m\ s^{-1}$)	L (m)	σ_θ (rad)	σ_ϕ (rad)	Ambient atmospheric stability
274140958	2.87	291.1°	−0.51	0.30	−13.4	0.27	0.14	B
274143957	2.56	292.1°	−0.53	0.28	−7.7	0.32	0.15	A
274150957	2.81	290.9°	−0.33	0.30	−11.7	0.33	0.15	B
274153956	2.98	291.7°	−0.25	0.30	−17.4	0.32	0.15	B
279080959	1.0	251.1°	0.41	0.03	2.6	0.21	0.09	F
279084000	0.97	246.7°	0.33	0.05	7.3	0.22	0.10	F
279090959	1.45	253.2°	−0.31	0.14	−30.5	0.27	0.14	C
279093959	1.82	250.1°	−0.35	0.18	−23.2	0.27	0.15	B
283081959	1.24	254.4°	0.02	0.10	58.8	0.29	0.11	E
283085000	0.95	263.2°	0.18	0.09	−146.4	0.26	0.12	D
283092000	1.12	241.6°	−0.43	0.11	−18.7	0.42	0.12	B
293103458	2.0	272.3°	−0.07	0.18	−133.3	0.23	0.13	D
293110458	2.10	271.3°	−0.11	0.20	−78.8	0.28	0.16	C
296080500	2.92	181.4°	0.10	0.24	62.3	0.15	0.09	E

In model simulations the computed velocity fields using (6a) compared poorly with the field data. In order to improve the model results a polynomial has been fitted to the wind tunnel measurements of velocity deficit shown in Fig. 6 yielding

$$T(\zeta) = b_0 + b_1\zeta + \cdots + b_6\zeta^5. \qquad (6b)$$

The coefficients are given in Table 2. The computed velocity fields for the GM experiment were greatly improved using (6b) as compared to (6a).

The turbulent Kinetic energy terms are given by

$$(\overline{u'^2}, \overline{v'^2}, \overline{w'^2}) \equiv (\langle\overline{u'^2}\rangle, \langle\overline{v'^2}\rangle, \langle\overline{w'^2}\rangle) = (a_1, a_2, a_3)A^2Q^2\bar{s}^{-1.2}F_c(\chi, \omega), \qquad (7)$$

where $\chi = y(W_d\bar{s}^{0.4})^{-1}$, $\omega = z(h\bar{s}^{0.4})^{-1}$ and u and v are oriented in the s and n directions, respectively. The constants a_1, a_2, a_3 were evaluated from wind tunnel data and were found to be 0.048, 0.040 and 0.30, respectively. Here F_c was determined by a least-squares orthogonal polynomial fit to wind tunnel data and is given by

$$F_c(\chi, \omega) = \sum_{n=0}^{4}\sum_{m=0}^{2} \psi_{n,2m}\omega^n\chi^{2m}, \qquad (8)$$

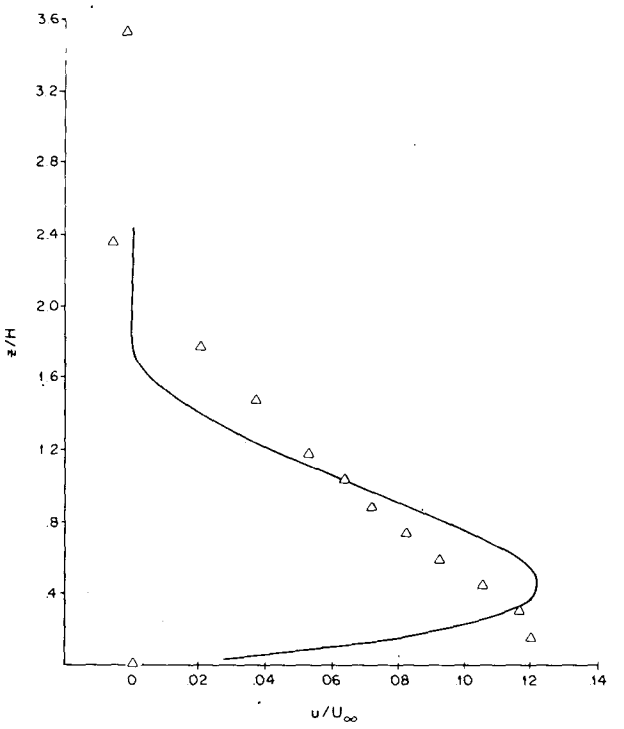

FIG. 6. Velocity deficit in vehicle wake, curve is the theoretical solution (6a) for the center line velocity deficit at $x/H = 30$ and deltas represent data taken by Eskridge and Thompson, (1982) in wind tunnel experiments.

TABLE 2. Constant for the polynomial fits in (6) and (8).

Surface fit		Curve fit	
Ψ_{00}	0.3511237×10^{-1}	b_0	0.0179349
Ψ_{01}	0.1255308×10^{2}		
Ψ_{02}	-0.4796241×10^{2}	b_1	2.5765870
Ψ_{03}	0.6732523×10^{2}		
Ψ_{04}	-0.3572466×10^{2}	b_2	−2.3062584
Ψ_{20}	−0.1890581	b_3	0.8951468
Ψ_{21}	-0.9345507×10^{1}		
Ψ_{22}	-0.1821427×10^{3}	b_4	−0.1758604
Ψ_{23}	0.5617911×10^{3}		
Ψ_{24}	-0.3995373×10^{3}	b_5	0.0169970
Ψ_{40}	0.2649465		
Ψ_{41}	-0.9434068×10^{2}	b_6	−0.0006404
Ψ_{42}	0.1034830×10^{4}		
Ψ_{43}	-0.2348153×10^{4}		
Ψ_{44}	0.1510437×10^{4}		

subject to the restriction that $F_c(\chi, \omega) \geq 0.0$. The constants in (8) are listed in Table 2.

The observed wind velocity fluctuations at some fixed point near a roadway are due to three distinct causes. Clearly, velocity fluctuations are produced by the wake turbulence described by (7) as well as by the ambient turbulence. Fluctuations will also occur because of the time variation in the wind velocity as a vehicle's wake passes the fixed point. This wake-passing effect is clearly *not* turbulence but an artifact arising due to the data being in the Eulerian rather than in the Lagrangian frame of reference.

To see how the wake-passing effect arises let us consider, as an example, the case in which a single vehicle moves very slowly through a laminar atmosphere with a wind velocity $u(z)$ normal to the road. An instrument at height z_0 along the roadway records a constant wind velocity of $u(z_0)$; the velocity rises smoothly and then falls back to $u(z_0)$ as the vehicle's wake passes the instrument. For a time period T, which is large compared to the period of wake passage, the average wind velocity is approximately $u(z_0)$. However, because $u(t) - u(z_0) = u'(t) \neq 0$, and hence $u'^2 \neq 0$, the laminar wake can be mistakenly identified as turbulent. One of the properties of turbulence is that it is diffusive. In the example given, however, the flow is clearly nondiffusive since it is laminar. This same phenomenon occurs in a turbulent atmospheric flow with turbulent wakes. However, in a "real world" roadway study where the vehicles are randomly distributed one will not be able to separate the wake-passing effect in the measured velocity variance from the ambient and wake turbulence as was possible with GM data. This pseudoturbulence must be accounted for in analysis of velocity data taken near a roadway.

Let the superscripts p, w and the subscript ∞ represent the wake-passing effect, the wake turbulence and the ambient turbulence, respectively. The total

velocity variance is assumed, as a first approximation, to be determined by adding the components so that

$$\overline{u'^2} = \overline{u'^2}^p + \overline{u'^2}^w + \overline{u'^2_\infty}, \tag{9}$$

with similar expressions for $\overline{v'^2}$ and $\overline{w'^2}$. It should be noted that Eq. (9) assumes there are no interactions between the various scales of turbulence. The velocity variance energy is defined by $\frac{1}{2}(\overline{u'^2} + \overline{v'^2} + \overline{w'^2})$ for the total variance with similar definitions for the ambient, wake, and wake-passing velocity variance. It should be noted that while the wake-passing turbulence can be very large, it is nondiffusive and one is interested in it only as a feature of the vehicle wake theory.

b. *Multi-vehicle velocity and turbulence fields*

The equations describing multivehicle wind velocity, turbulence and wake-passing effect are presented below. The derivations for these equations are presented in the appendix.

The horizontal wind velocity components are computed by

$$\left.\begin{aligned}\langle\overline{u(\mathbf{x}_0, t)}\rangle &= \overline{U_\infty(z_0, t)} - \frac{1}{TV_h} \\ &\times \sum_{j=1}^{N} \int_{-TV_h/2}^{TV_h/2} \left\langle u_{D_j}\left(\mathbf{x}_0, \frac{y}{V_h}\right)\right\rangle \sin\alpha_j dy \\ \langle\overline{v(\mathbf{x}_0, t)}\rangle &= \overline{V_\infty(z_0, t)} - \frac{1}{TV_h} \\ &\times \sum_{j=1}^{N} \int_{-TV_h/2}^{TV_h/2} \left\langle u_{D_j}\left(\mathbf{x}_0, \frac{y}{V_h}\right)\right\rangle \cos\alpha_j dy\end{aligned}\right\}, \tag{10}$$

where V_h is the average vehicle speed, $\mathbf{x}_0 = (x_0, y_0, z_0)$, $\langle u_{D_j}\rangle$ is given by (4), N is the number of vehicle passing the point $\mathbf{x}_0$ during time interval $(-T/2, T/2)$ and α is the angle between the relative wind $\mathbf{Q}$ and the highway, and U_∞, V_∞ represent the upwind ambient conditions.

The turbulent kinetic energy component along the x axis is given by

$$\langle\overline{u'^2(\mathbf{x}_0, t)}^w\rangle = \frac{1}{TV_h} \sum_{j=1}^{N} \int_{-TV_h/2}^{TV_h/2} \overline{\left\langle u'^2_w\left(\mathbf{x}_0, \frac{y}{V_h}\right)\right\rangle} dy, \tag{11}$$

where $\langle\overline{u'^2_w}\rangle$ is given by (7) and similar expressions are found for $\langle\overline{v'^2}^w\rangle$ and $\langle\overline{w'^2}^w\rangle$.

The velocity variance due to wake passing is given by

$$\left\{\begin{matrix}\langle\overline{u'^2(\mathbf{x}_0, t)}^p\rangle \\ \langle\overline{v'^2(\mathbf{x}_0, t)}^p\rangle\end{matrix}\right\} = \frac{1}{TV_h} \sum_{j=1}^{N} \int_{-TV_h/2}^{TV_h/2} \left[\left\langle U_j\left(\mathbf{x}_0, \frac{y}{V_h}\right)\right\rangle \times \left\{\begin{matrix}\sin\alpha_j \\ \cos\alpha_j\end{matrix}\right\} - \left\{\begin{matrix}\langle\overline{u(\mathbf{x}_0, t)}\rangle \\ \langle\overline{v(\mathbf{x}_0, t)}\rangle\end{matrix}\right\}\right]^2 dy, \tag{12}$$

where $U_j = |(\bar{U}_\infty, \bar{V}_\infty)| - \langle u_{D_j}\rangle$. Eqs. (10), (11) and (12) are integrated by use of Simpson's method.

5. Results

As shown in Section 3 the autocorrelograms of the fluctuating wind velocity components in the GM experiment show a distinct 29 s oscillation due to the passage of the vehicle groups past the tower line at 29 s intervals. In Fig. 4, the average fluctuating wind velocities using (3) from the 1.5 m elevation sites are plotted for case 293110458. This 29 s wave contains almost exclusively the energy due to wake passing and has a nondiffusive effect on pollutants emitted by vehicles. The vertical component ($\hat{w}'$) of the 29 s wave in this data set is only detectable immediately next to the road. The $\hat{u}'$ (along wind) component is clearly detectable 15 m from the road, and the $\hat{v}'$ (crosswind) component is clearly evident 50 m downwind of the road.

The kinetic energy in the wake-passing effect has been estimated from the GM data by use of (3) and is plotted in Fig. 7 against travel time. Fig. 8 shows the wake effect as seen in the 30-min averaged fields (see also Fig. 13 in Eskridge and Hunt, 1979). In Fig. 8, the direction of the traffic is clearly seen in the $\bar{v}$

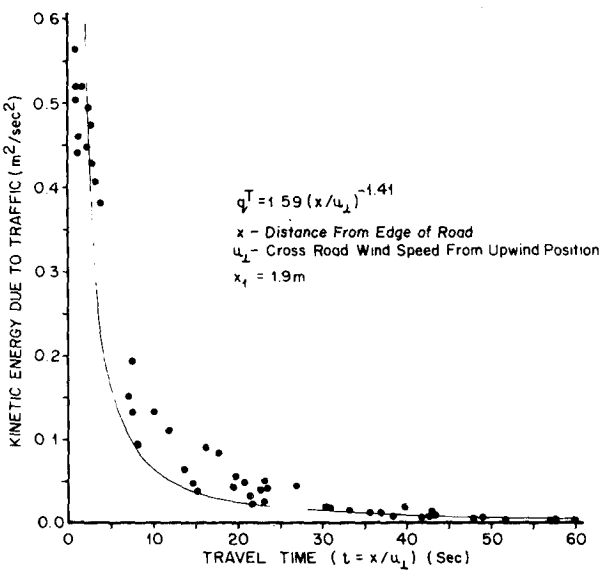

FIG. 7. Plot of the kinetic energy associated with the 29 s wave versus travel time.

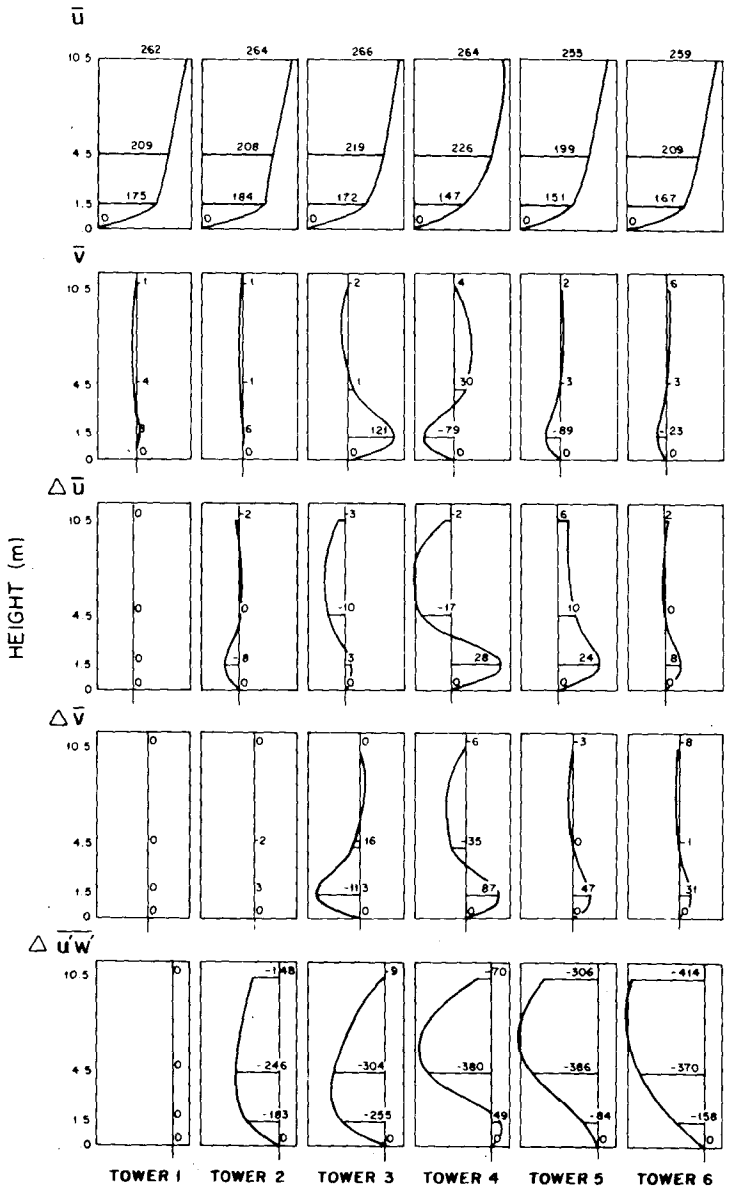

FIG. 8. Thirty-minute averaged wind and turbulence components for case 2931104 for each wind instrument on each of the six towers. Units are cm s^{-1} and $cm^2 s^{-2}$. Except for the horizontal wind components $\bar{u}$ and $\bar{v}$, the upwind values have been subtracted from each value to give an approximate wake result.

field and the velocity changes due to the wakes of the vehicles can be seen in the $\bar{\Delta}u$ ($\bar{\Delta}u = \bar{u} - \bar{u}_\infty$) and $\bar{\Delta}v$ ($\bar{\Delta}u = \bar{v} - \bar{v}_\infty$) fields. The Reynolds stress fields are strongest near the road, as expected, with the wake effects clearly visible at tower 6 in several of the fields of values of Reynolds stresses.

The observed velocity variance energy, the observed velocity variance energy minus ambient, the energy computed from (3), the wake-passing effect computed from (12), and the wake turbulence computed from (11) are shown in Table 3 for case 293110458 at sites 12, 15, 18, 19 and 20 (see Fig. 1). At site 12, the energy in the analyzed 29 s wave is 60% of the observed-minus-ambient value and further from the roadway is a significant portion of the observed velocity variance energy or exceeds the observed-minus-ambient estimate. Similar results found for the other cases listed in Table 1 are not shown.

The results shown in Table 3, which are typical of all GM experiments, imply that the measured velocity variance consists mainly of that energy due to wake-passing, which is pseudoturbulence. The values in Table 3 show that the model predictions for both wake turbulence and wake-passing effect are larger

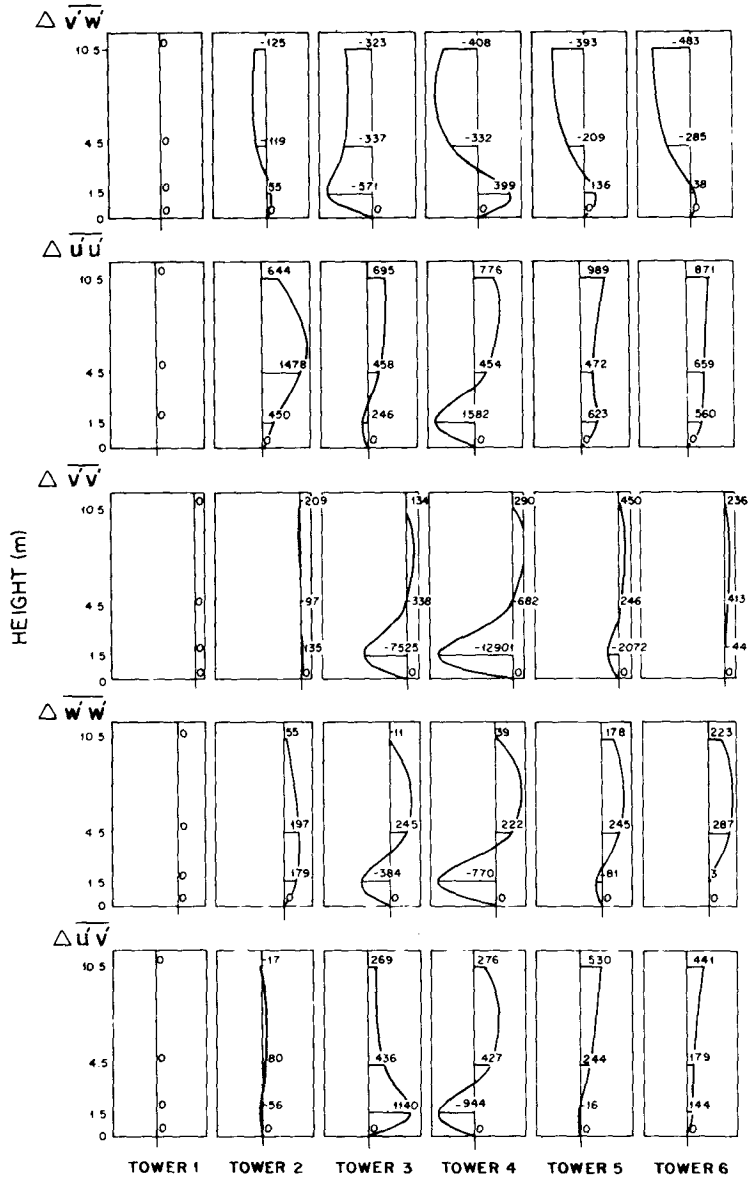

FIG. 8. (*Continued*)

than the analyzed wake-passing effect and wake turbulence. The negative values found in Table 3 imply that the turbulence is not a linear process as assumed by (9).

One possible reason for the difference between the model predictions of velocity variance and the observed data is that the velocity changes and turbulence of each individual vehicle wake of the vehicle groups occur at a frequency that cannot be resolved using Gill anemometers. It is easy to demonstrate that sampling every second underestimates the velocity variance due to wake turbulence and wake-passing. This accounts, in part, for the large difference in the observed and the model results shown in Table 3. For example, the wake width (of a typical 1975 American car) is approximately 3 m (Eskridge and Thompson, 1982). With a cross wind speed $u = 0.3$ m s^{-1} and sampling once per second, the resulting resolution is 10 points across a single wake. The turbulent eddies in the wake are much smaller than 3 m and hence will not be resolved correctly in this example because it is necessary to sample 10 times per cycle in order to resolve 95% of the energy of a wave [Fig. 2.2 of Pasquill (1974) shows the effect of averaging over a time s on the variance of a wave frequency n]. However, decreasing the sampling time is equivalent to increasing the sampling rate, even though the velocity profile will be adequately sampled in this example. Clearly, when $u \geq 1.0$ m s^{-1}, the

TABLE 3. The turbulent kinetic energy from observations, observations minus background, from the 29-s waves, from model prediction and model predictions of wake passing in $m^2 s^{-2}$ for case 293110458.

Site	Observed	Observed minus background	Analyzed wake passing (3)	Observed wake turbulence	Computed wake passing (12)	Computed wake turbulence (11)
12	1.102	0.801	0.483	0.318	0.79	1.26
15	0.416	0.115	0.138	−0.023	0.20	0.28
18	0.313	0.012	0.051	−0.039	0.12	0.15
19	0.275	−0.026	0.018	—	0.08	0.09

velocity changes due to the wake will not be sampled sufficiently.

When the velocity change due to a vehicle (u_{D_j}) is not correctly resolved, (12) shows that the wake-passing velocity variance will not be correctly resolved. A spectral analysis of data taken in the wake of a block car (simulating a pure momentum wake) showed that the most energetic eddies have a length of about 1 m (results not shown), and three data points (as in the above example) will not resolve the energy in eddies of this size. For a crosswind speed of 5 m s^{-1}, the minimum number of samples needed to resolve the 1 m eddy is 50 samples per second. Doubling the sample rate is advisable in order to resolve smaller eddies, which may contain a significant amount of wake turbulent energy near a roadway. A sampling rate of 100 per second requires, of course, an anemometer with a very fast response time.

From the above discussion, it is evident that the GM wind velocity measurements are not of sufficient resolution to determine wake turbulence. The agreement that Eskridge and Hunt (1979) found between the model computations of the turbulent kinetic energy components and the GM data was spurious. Eskridge and Hunt used the meteorological data from eight experiments in which the SF_6 data were erroneous to calibrate their model (i.e. to determine γ, a_0, a_1, and a_2). Hence, the computed values of $\overline{u'^2}$, $\overline{v'^2}$ and $\overline{w'^2}$ included wake turbulence and wake-passing effect and not just wake turbulence; this was also true for the results presented in Sedefian *et al.* (1981).

The results of Chock (1978b), who determined the magnitude of the component of the eddy diffusivity tensor K_{ij} using the GM data, are also suspect because of the data resolution and Chock was not aware that the wake-passing effect will dominate the observed velocity variances.

The contention that the GM data are not resolving the wake properly is also supported by the spectral analysis of Chock (1980). Chock's Fig. 6d shows that the energy downwind of the roadway increases as frequency increases at 0.5 Hz (as wavelength decreases), the Nyquist frequency, indicating the eddies containing the most energy have not been properly resolved in the data. While aliasing will fold some of the energy of the wave of frequency greater than 0.5 Hz into lower frequencies the energy in the entire spectrum is underestimated. The results of Rao *et al.* (1979) (see their Fig. 4d) show that a significant portion of traffic-induced velocity variance will be in eddies of frequency greater than 0.5 Hz.

Fig. 9 is a plot of the vertical profiles of velocity deficit for a 1/32 scale vehicle taken in wind tunnel experiments by Eskridge and Thompson at various distances downwind of the vehicle. In the GM experiment anemometers were located at 1.5, 4.4 and 10.4 m above the surface. Fig. 9 shows that only one of these instruments will be in the wake. In order to resolve the wake in the vertical direction, anemometers should be located at 0.25, 0.75, 1.25, 1.75, 2.25 m above the ground.

In order to accurately predict wake-passing effect, it is necessary to predict the changes in the wind field caused by the moving vehicles. Of the two horizontal

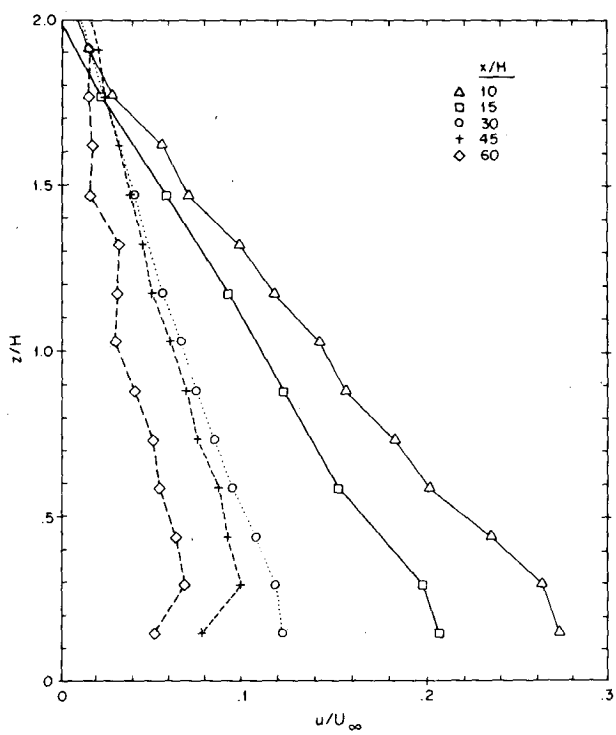

FIG. 9. Vertical profiles of velocity deficit for 1/32 scale vehicle along the centerline of the vehicle wake (from Eskridge and Thompson, 1982).

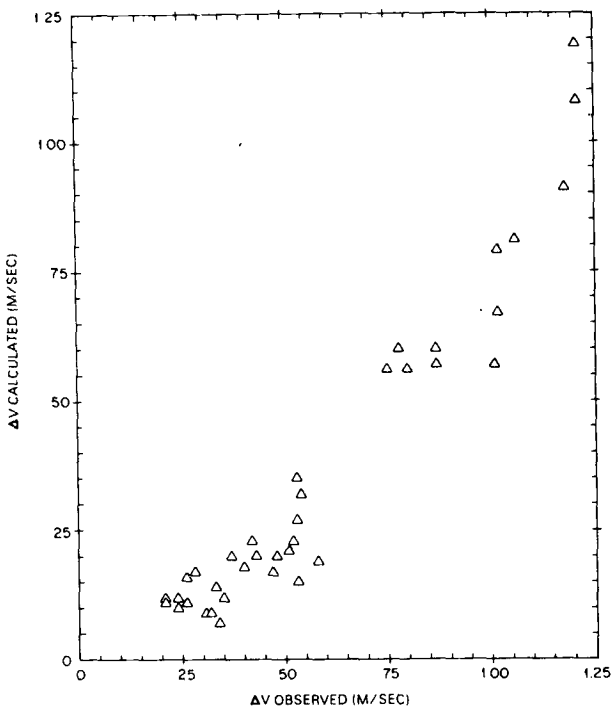

FIG. 10. Plot of observed velocity change ($\Delta\bar{v} = \bar{v}_\infty - \bar{v}$) versus computed velocity change.

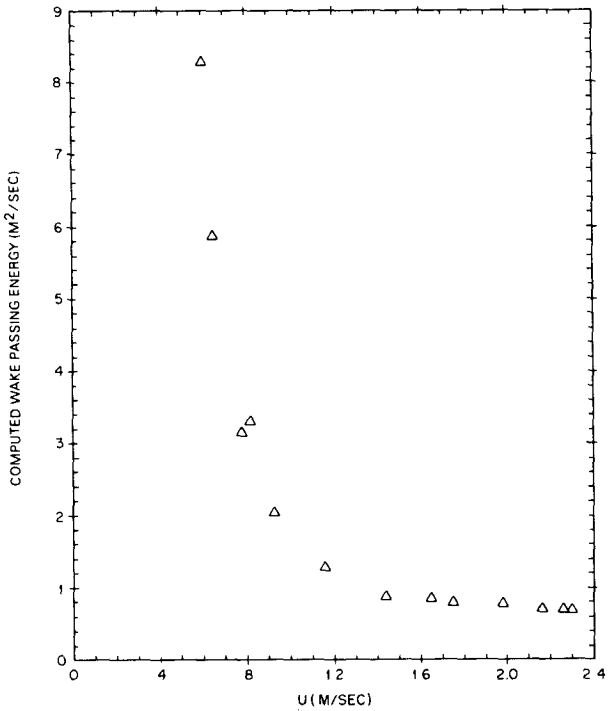

FIG. 11. Model predictions of wake-passing effect versus the normal component of the wind velocity at site 12.

wind components, the component parallel to the road (v-component) is most affected, as shown in Fig. 8. Figure 10 is a plot of the observed versus model prediction of the v component of the velocity at sites 12, 15 and 18 downwind of the road. Fig. 10 shows that model predictions of velocity changes near the roadway are somewhat less than the values observed. With smaller value of wind speed $\bar{u}$ and $\bar{v}$, (12) implies that the wake-passing components of $\overline{u'^2}^p$ and $\overline{v'^2}^p$ will be slightly underestimated. However, as Fig. 11 and Fig. 7 show, the predicted wake-passing turbulence calculated from (12) is much larger than the observed as determined by (3). The computed wake-passing effect, when plotted against time, does not decay at the same rate as the observed wake-passing effect does as shown in Fig. 7.

The computed wake-passing effect is seen (Fig. 11) to be highly dependent on crossroad wind speed below a speed of 1.4 m s^{-1} and essentially constant for higher crosswind speeds. For sufficiently high crosswind speeds each vehicle wake is independent. From Fig. 11 one can infer that the error, by ignoring other vehicles and treating each vehicle as if it is not affected by other vehicles, is small when the crosswind speed is greater than 1.4 m s^{-1}. For comparative purposes, the predicted wake turbulent kinetic energy is plotted in Fig. 12 for site 12 as a function of wind speed. The wake kinetic energy is seen in this figure to increase linearly with wind speed.

The difference between the model results and the observations may not be due only to the fact that the data do not properly resolve the velocity changes and high frequency turbulent eddies. The vehicles in the

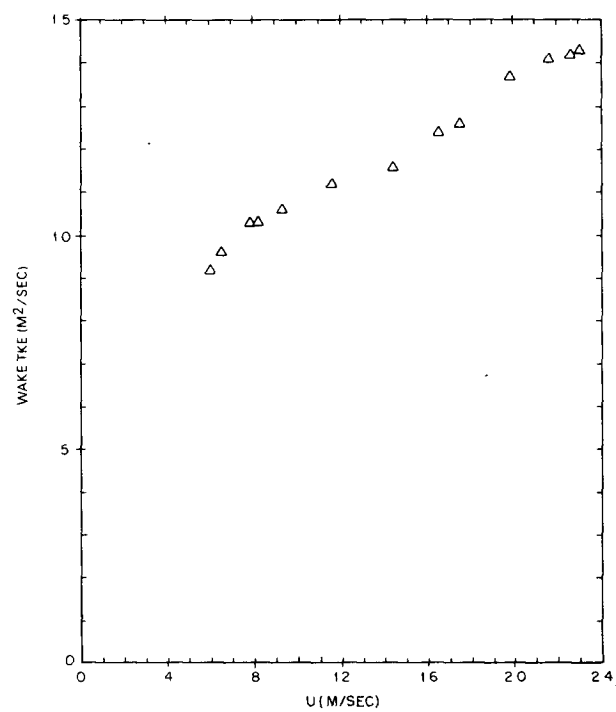

FIG. 12. Plot of model-predicted wake turbulent kinetic energy versus the normal component of the wind velocity at site 12.

GM experiment traveled in packs in which the cars were separated by approximately two car lengths. Under these conditions, treating each vehicle as if it were not affected by other vehicles introduces an error of unknown magnitude [however for a cross wind speed > 2.0 m s^{-1} the error should be small]. Secondly, modern streamlined automobiles have lift, which induces a vortex wake, thus modifying the momentum wake by mixing ambient air into the wake and also spreading the wake. Finally the wake-passing computation is subject to error because the summation terms in (10) require the computation of small differences in large numbers (the interaction of the north and south bound lanes). Errors arising from (10) can be magnified in (12) when the velocity variance components are calculated. While it is not possible to quantify these errors, they are probably small.

6. Summary and conclusions

This study has shown that the velocity variances observed in the GM experiment were dominated by the wake-passing effect and that spacial and temporal resolutions of the data were inadequate to resolve the wake-turbulence effects. For reasonable accuracy the maximum sampling rate for Gill anemometers is about one per second. Because of the limitations of these instruments the GM data base cannot be used directly to validate the vehicle wake model described in this paper. The values of wake-passing effect extracted from the data by (3) lend support to the model predictions. The measured concentration data of GM experiment are, of course, unaffected by the wake-passing effect and show the true diffusion of the tracer due to ambient and vehicle wake turbulence. The GM SF_6 data has been used by Rao and Keenan (1980) to derive a new set of diffusion curves for a Gaussian model. The model predictions of pollutant concentration were a significant improvement over previous models using different diffusion curves.

The wind data in the GM experiment gave a qualitative picture of the effect of vehicle wakes on the velocity and turbulence fields. However, it is recommended in future experiments that either fast-response anemometers be used so that the wake effect can be accurately resolved or slow-response anemometers be used only to determine the upwind ambient conditions.

Recommendations are made, based on wind tunnel experiments and modeling results as to the time resolution and spacing that are necessary to resolve vehicle wake turbulence.

Acknowledgments. One of the authors (S. T. Rao) acknowledges the support of the U.S. Environmental Protection Agency under Grant R-806017-01. We acknowledge the drafting of the figures by Carol Clas and Gary Lanphear, and Eileen Ward for typing the manuscript. We also acknowledge the detailed and constructive criticism of the referees which improved the paper.

APPENDIX

Velocity Field Development

Consider the case of one vehicle moving down a roadway with speed V_h. The time averaged horizontal wind velocity measured at a point $\mathbf{x}_0 = (x_0, y_0, z_0)$ downwind of the roadway during the time interval $[-T/2, T/2]$ for a large number of experiments (ensemble average) is represented by $\langle\overline{u(\mathbf{x}_0, t)}\rangle$ and $\langle\overline{v(\mathbf{x}_0, t)}\rangle$. Each wind component consists of the ensemble, time-averaged ambient wind $\langle\overline{U_\infty(z_0, t)}\rangle$ and $\langle\overline{V_\infty(z_0, t)}\rangle$ plus the change in the average the wind velocity due to the wake of the vehicle and can be written in component form as

$$\left.\begin{aligned}\langle\overline{u(\mathbf{x}_0, t)}\rangle &= \overline{U_\infty(z_0, t)} \\ &\quad - \left\langle\frac{1}{T}\int_{-T/2}^{T/2} u_D(\mathbf{x}_0, t)\sin\alpha dt\right\rangle \\ \langle\overline{v(\mathbf{x}_0, t)}\rangle &= \overline{V_\infty(z_0, t)} \\ &\quad - \left\langle\frac{1}{T}\int_{-T/2}^{T/2} u_D(\mathbf{x}_0, t)\cos\alpha dt\right\rangle\end{aligned}\right\}, \quad \text{(A1)}$$

where u_D represents the velocity change at point x_0 due to the passage of the vehicle wake (at this point the functional form of u_D is unknown) and α is the angle between the road and the relative wind $\mathbf{Q}$ acting on the vehicle and it assumed that $\langle\overline{U(z_0, t)}\rangle = \overline{U_\infty(z_0, t)}$.

It is assumed that the vehicle speed is much greater than the ambient windspeed and that the time that the influence of the wake from a single vehicle is felt at point $\mathbf{x}_0$ is much less than the time interval T. The last assumption implies that for N vehicles passing point $\mathbf{x}_0$ during time interval $[-T/2, T/2]$ the average velocity is given by summing the effect of each of the N vehicles, that is

$$\left.\begin{aligned}\langle\overline{u(\mathbf{x}_0, t)}\rangle &= \overline{U_\infty(z_0, t)} \\ &\quad - \left\langle\sum_{j=1}^{N}\frac{1}{T}\int_{-T/2}^{T/2} u_{D_j}(\mathbf{x}_0, t)\sin\alpha_j dt\right\rangle \\ \langle\overline{v(\mathbf{x}_0, t)}\rangle &= \overline{V_\infty(z_0, t)} \\ &\quad - \left\langle\sum_{j=1}^{N}\frac{1}{T}\int_{-T/2}^{T/2} u_{D_j}(\mathbf{x}_0, t)\cos\alpha_j dt\right\rangle\end{aligned}\right\}. \quad \text{(A2)}$$

Equation (A2) is not in a form that lends itself to a direct solution, so let $t = y/V_h$. Then (A2) can be written as

$$\left.\begin{aligned}\langle\overline{u(\mathbf{x}_0,t)}\rangle &= \overline{U_\infty(z_0,t)} - \frac{1}{TV_h}\\ &\times \sum_{j=1}^{N}\int_{-TV_{h/2}}^{TV_{h/2}} \langle u_{D_j}(\mathbf{x}_0, y/V_h)\rangle \sin\alpha_j dy\\ \langle\overline{v(\mathbf{x}_0,t)}\rangle &= \overline{V_\infty(z_0,t)} - \frac{1}{TV_h}\\ &\times \sum_{j=1}^{N}\int_{-TV_{h/2}}^{TV_{h/2}} \langle u_{D_j}(\mathbf{x}_0, y/V_h)\rangle \cos\alpha_j dy\end{aligned}\right\}, \quad \text{(A3)}$$

which is Eq. (10) in the text.

The average wind field for the period $[-T/2, T/2]$ can now be determined from (A3), since the change in velocity due to each vehicle wake u_{D_j} is now a function of position only and is given by (4). Equation (A3) is integrated by Simpson's method to calculate the velocity at point $\mathbf{x}_0$. Usually, limits much smaller than $TV_h/2$ can be used to evaluate (A3), since u_{D_j} decreases as $\bar{s}^{-0.75}$, implying that the error made when using different integration limits is very small.

The turbulent kinetic energy calculated from observations at point $\mathbf{x}_0$ due to the wake turbulence of a single passing vehicle is found from

$$\langle\overline{u'^2(\mathbf{x}_0,t)}^{w}\rangle = \langle\frac{1}{T}\int_{-T/2}^{T/2}\overline{u_w'^2(\mathbf{x}_0,t)}dt\rangle, \quad \text{(A4)}$$

where $\overline{u_w'^2(\mathbf{x}_0,t)}$ is a functional form representing the wake turbulence with similar forms for $\overline{v'^2}^{w}$ and $\overline{w'^2}^{w}$. As before setting $t = y/V_h$ for N vehicles yields

$$\langle\overline{u'^2(\mathbf{x}_0,t)}^{w}\rangle = \frac{1}{TV_h}\sum_{j=1}^{N}\int_{-TV_{h/2}}^{TV_{h/2}}\langle\overline{u_w'^2(\mathbf{x}_0,y/V_h)}\rangle dy \quad \text{(A5)}$$

and $\langle\overline{u_w'^2(\mathbf{x}_0,y/V_h)}\rangle$ is given by (7). Similar expressions are found for $\overline{v'^2}^{w}(\mathbf{x}_0,t)$ and $\overline{w'^2}^{w}(\mathbf{x}_0,t)$. Equation (A5) is integrated using Simpson's method and is (11) in the text.

The wake-passing effect arises out of the change in the velocity field due to the vehicle wake which appears in the data recorded at a fixed point, upon time averaging, as turbulent kinetic energy.

For a single vehicle, the wake-passing effect at point $\mathbf{x}_0$ would be

$$\begin{Bmatrix}\langle\overline{u'^2(\mathbf{x}_0,t)}^{p}\rangle\\ \langle\overline{v'^2(\mathbf{x}_0,t)}^{p}\rangle\end{Bmatrix} = \frac{1}{T}\int_{-T/2}^{T/2}\left[\langle U(\mathbf{x}_0,t)\rangle\begin{Bmatrix}\sin\alpha\\ \cos\alpha\end{Bmatrix} - \begin{Bmatrix}\langle\overline{u(\mathbf{x}_0,t)}\rangle\\ \langle\overline{v(\mathbf{x}_0,t)}\rangle\end{Bmatrix}\right]^2 dt, \quad \text{(A6)}$$

where

$$\langle U(\mathbf{x}_0,t)\rangle = |(\bar{U}_\infty, \bar{V}_\infty)| - \langle u_D(\mathbf{x}_0,t)\rangle.$$

As before, changing the variables ($t = y/V_h$) and summing for N vehicles leads to a more tractable form

$$\begin{Bmatrix}\langle\overline{u'^2(\mathbf{x}_0,t)}^{p}\rangle\\ \langle\overline{v'^2(\mathbf{x}_0,t)}^{p}\rangle\end{Bmatrix} = \frac{1}{TV_h}\sum_{j=1}^{N}\int_{-TV_{h/2}}^{TV_{h/2}}\left[\langle U_j\left(\mathbf{x}_0,\frac{y}{V_h}\right)\rangle \times \begin{Bmatrix}\sin\alpha_j\\ \cos\alpha_j\end{Bmatrix} - \begin{Bmatrix}\langle\overline{u(\mathbf{x}_0,t)}\rangle\\ \langle\overline{v(\mathbf{x}_0,t)}\rangle\end{Bmatrix}\right]^2 dy, \quad \text{(A7)}$$

where

$$U_j = |(\bar{U}_\infty, \bar{V}_\infty)| - \langle u_{D_j}\rangle.$$

There is a vertical component to the wake-passing effect but it is small as the data show (see Section 5) and the Eskridge and Hunt theory assumes it to be zero.

Equation (A7) is integrated by Simpson's method where the ensemble average inside the integral is determined by (A3) and (4).

REFERENCES

Cadle, S. H., D. P. Chock, J. M. Heuss and P. R. Monson, 1976: Results of the General Motors sulfate dispersion experiments. General Motors Res. Publ. GMR-2107, Warren, MI, 140 pp.

Chock, D. P., 1977: The General Motors sulfate dispersion experiment: An overview of the wind, temperature and concentration fields. *Atmos. Environ.*, **11**, 553–559.

——, 1978a: A simple line-source model for dispersion near roadways. *Atmos. Environ.*, **12**, 823–829.

——, 1978b: An advection–diffusion model for pollutant dispersion near roadways. *J. Appl. Meteor.*, **17**, 976–989.

——, 1980: General Motors Sulfate Dispersion Experiment—An analysis of the wind field near a road. *Bound.-Layer Meteor.*, **18**, 431–451.

Eskridge, R. E., and J. C. R. Hunt, 1979: Highway modeling. Part I: Prediction of velocity and turbulence fields in the wakes of vehicles. *J. Appl. Meteor.*, **18**, 387–400.

——, and R. S. Thompson, 1982: Experimental and theoretical study of the wake of a block-shaped vehicle in a shear-free boundary flow. *Atmos. Environ.*, **16**, 2821–2836.

——, F. S. Binkowski, J. C. R. Hunt, T. L. Clark and K. L. Demerjian, 1979: Highway modeling. Part II: Advection and diffusion of SF_6 tracer gas. *J. Appl. Meteor.*, **18**, 401–412.

Pasquill, F., 1974: *Atmospheric Diffusion.* Wiley and Sons, 429 pp.

Rao, S. T., and M. Keenan, 1980: Suggestions for the improvement of the EPA-HIWAY model. *J. Air Pollut. Control Assoc.*, **30**, 247–256.

——, L. Sedefian and U. Czapski, 1979: Characteristics of turbulence and dispersion of pollutants near major highways. *J. Appl. Meteor.*, **18**, 283–293.

——, G. Sistla, M. T. Keenan and J. S. Wilson, 1980: An evaluation of some commonly used highway dispersion models. *J. Air Pollut. Control Assoc.*, **30**, 239–246.

Sedefian, L., 1977: Some characteristics of turbulence adjacent to a major highway, M.S. thesis, State University of New York at Albany, 44 pp.

——, S. T. Rao and U. Czapski, 1981: Effects of traffic-generated turbulence on near-field dispersion. *Atmos. Environ.*, **15**, 527–536.

Tennekes, H., and J. L. Lumley, 1972: *A First Course in Turbulence,* MIT Press, 300 pp.

Zimmerman, J. R., and R. S. Thompson, 1975: User's Guide for HIWAY, a highway air pollution model. Rep. No. EPA-650/4-74-008, 59 pp.